JMB

Available online at www.sciencedirect.com

ScienceDirect

ELSEVIER

Cysteine as a Modulator Residue in the Active Site of Xenobiotic Reductase A: A Structural, Thermodynamic and Kinetic Study

Olivia Spiegelhauer[1], Sophia Mende[1], Frank Dickert[2], Stefan H. Knauer[1], G. Matthias Ullmann[2] and Holger Dobbek[1]*

[1]*Bioinorganic Chemistry, Universität Bayreuth, Universitätsstrasse 30, 95447 Bayreuth, Germany*

[2]*Structural Biology/ Bioinformatics, Universität Bayreuth, Universitätsstrasse 30, 95447 Bayreuth, Germany*

Xenobiotic reductase A (XenA) from *Pseudomonas putida* 86 catalyzes the NADH/NADPH-dependent reduction of various substrates, including 2-cyclohexenone and 8-hydroxycoumarin. XenA is a member of the old yellow enzyme (OYE) family of flavoproteins and is structurally and functionally similar to other bacterial members of this enzyme class. A characteristic feature of XenA is the presence of a cysteine residue (Cys25) in the active site, where in most members of the OYE family a threonine residue is found that modulates the reduction potential of the FMN/FMNH⁻ couple. We investigated the role of Cys25 by studying two variants in which the residue has been exchanged for a serine and an alanine residue. While the exchange against alanine has a remarkably small effect on the reduction potential, the reactivity and the structure of XenA, the exchange against serine increases the reduction potential by +82 mV, increases the rate constant of the reductive half-reaction and decreases the rate constant in the oxidative half-reaction. We determined six crystal structures at high to true atomic resolution (d_{min} 1.03–1.80 Å) of the three XenA variants with and without the substrate coumarin bound in the active site. The atomic resolution structure of XenA in complex with coumarin reveals a compressed active site geometry in which the isoalloxazine ring is sandwiched between coumarin and the protein backbone. The structures further reveal that the conformation of the active site and substrate interactions are preserved in the two variants, indicating that the observed changes are due to local effects only. We propose that Cys25 and the residues in its place determine which of the two half-reactions is rate limiting, depending on the substrate couple. This might help to explain why the genome of *Pseudomonas putida* encodes multiple xenobiotic reductases containing either cysteine, threonine or alanine in the active site.

© 2010 Elsevier Ltd. All rights reserved.

Keywords: aromatic degradation; *Pseudomonas putida*; old yellow enzyme; flavin; FMN

Edited by R. Huber

Introduction

Xenobiotic reductases catalyze the NAD(P)H-dependent reduction of the olefinic bond of different α,β-unsaturated carbonyl compounds, including ketones and esters, and belong to the old yellow enzyme (OYE) family. Members of this family have been found in bacteria, yeasts, plants and nematodes,[1] and their physiological functions are mostly unknown. The genome of several bacteria contain multiple open-reading-frames encoding OYE homologs,[2,3] and the largest number of different OYE homologs are present in the genome of *Pseudomonas putida* KT2440, which encodes six variants named XenA – XenF.[4] On the basis of amino acid sequence alignments, these variants can be related to different subgroups of the

*Corresponding author. Institut für Biologie, Strukturbiologie/Biochemie, Humboldt-Universität zu Berlin, 10115 Berlin, Germany. E-mail address: Holger.Dobbek@uni-bayreuth.de.

Abbreviations used: OYE, old yellow enzyme; RHR, reductive half-reaction; OHR, oxidative half-reaction; MC, Monte Carlo.

OYE family and are likely to have evolved from different ancestors. XenA isolated from *P. putida* 86 was recently shown to be involved in the degradation of quinoline[5] along the 8-hydroxycoumarin pathway due to its ability to reduce the C3=C4 double bond of 8-hydroxycoumarin and its abundance, when *P. putida* 86 is grown in the presence of quinoline.[6] It shares the highest sequence identity with XenA, XenD and XenE from *P. putida* KT2440 and YqjM from *Bacillus subtilis*.[4] The crystal structure of XenA has been solved for the oxidized enzyme alone and with two substrates bound to the active site at a resolution of 1.5 Å.[6] XenA is a homodimer in solution and the crystal, and one FMN molecule is bound to each monomer. The subunit structure is similar to that reported for OYE,[7] morphinone reductase[8], PETN reductase[9,10], *Shewanella* yellow enzyme 1[11] and YqjM.[12] They all consist of the typical $(\beta/\alpha)_8$ barrel and FMN is bound at the C-terminal end. The *re* side of the flavin is facing the protein and the *si* side defines the bottom of a wide active site pocket. The reaction of XenA is consistent with a ping pong mechanism and can be divided into two half-reactions. A kinetic investigation using NADH and NADPH as substrates in the reductive half-reaction and 2-cyclohexenone and coumarin in the oxidative half-reaction revealed that either half-reaction can be rate-limiting, depending on the combination of substrates. In the reductive half-reaction the enzyme is reduced efficiently by NADPH, while the reaction with NADH is about 20-fold slower. The first step in this reaction is the formation of a charge transfer complex between the flavin cofactor and the nicotinamide, which is followed by a hydride transfer from NAD(P)H to FMN. In the oxidative half-reaction the enzyme can reduce different α,β-unsaturated carbonyl compounds. In this case we assume two different intermediates before the equivalents of two electrons and two protons are transferred on the substrate, suggesting that the relative orientations of FMN and the substrate changes from the encounter complex to the reactive complex. The rate constants for reductive and oxidative half-reactions are dependent on the reduction potential of the flavin cofactors.[13] The reduction potential of the FMN/FMNH⁻ couple in XenA was previously determined to be –263 mV,[13] which is considerably lower than the values found for other members of the OYE family.[14–16] XenA shows several structural variations that can be responsible for the difference in the reduction potential. One is a cysteine residue (Cys25) in the active site, which replaces a highly conserved threonine residue. The side chains of cysteine in XenA and the threonine residue are within hydrogen bonding distance to the O(4) carbonyl oxygen atom of the isoalloxazine ring. Mutagenesis studies of this threonine residue (Thr37 in OYE[17] and Thr32 in morphinone reductase[15)]) indicated that this residue modulates the flavin reduction potential. Cys26 in YqjM, which is analogous to Cys25 in XenA, was shown to adopt several conformations

interacting either with O(4) or with N(5) and might interact with the delocalized ring electrons of the adjacent Tyr28. It is therefore assumed that Cys26 acts as a redox sensor that is able to control the reduction potential of FMN, depending on the presence of substrates.[12] The exchange of Cys26 (C26D and C26G) altered the reactivity of YqjM and changed its enantioselectivity.[18]

The recent structural[6] and kinetic[13] studies of XenA did not reveal the contributions of individual active site residues. To gain insight into the role of Cys25 we studied its effect on the structure, the stabilization of substrate complexes and the kinetics of the catalytic cycle. We report the crystal structures of XenA and variants in which Cys25 has been replaced by alanine and serine with and without substrate bound in the active site, as well as the effect of the mutations on ligand binding and the kinetics of XenA. Threonine is the most frequently encountered amino acid at the position of Cys25 in related flavoenzymes. An inspection of the crystal structure of XenA reveals that the methyl group of threonine in a C25T variant of XenA would clash with the neighboring tyrosine residue (Tyr27) and we therefore preferred the exchange of cysteine for serine and cysteine for alanine. Our earlier structural characterization of XenA at a resolution of 1.5 Å indicated a deviation of the isoalloxazine ring from planarity; however, the interatomic distances within the active site, which contribute to create this strained conformation, could not be determined reliably.[6] We therefore extended our analysis to true atomic resolution (d_{min} 1.03 Å) to reveal the individual contributions to the deformation of the flavin. Our earlier analysis showed that Cys25 is close to the substrate-binding site but did not reveal any direct interaction between the residue and the substrate.[6] We were specifically interested in whether Cys25 would contribute to the stabilization of an intermediate or transition state of the reaction in comparison to the unreacted substrate to accelerate the overall reaction. The stabilization of a transition state cannot be revealed by a crystal structure, so we analyzed the kinetics of the two half-reactions of the XenA variants and compare it to that of the wild type protein.

Results and Discussion

Mutagenesis

The QuickChange mutagenesis protocol from Stratagene was used to mutate Cys25 in XenA wild type. PCR primers were designed to exchange this cysteine with alanine and with serine, and gene sequencing of the resulting expression plasmids confirmed the correct single site mutations. Both variants could be expressed and purified like the wild type enzyme. Mutagenesis did not result in a loss of FMN and all enzymes have an FMN content of 70 – 80%.

Spectroscopic properties and specific activity

Wild type Xen (XenA-wt), XenA-C25A and XenA-C25S showed only small differences in their absorbance spectra. The maximum peak of FMN was shifted from 464 nm in the wild type protein to 456 nm in XenA-C25A and to 460 nm in XenA-C25S (Supplementary Data Fig. S1). The extinction coefficients for the two peaks ($\varepsilon_{456} = 12.7$ mM^{-1} cm^{-1}; $\varepsilon_{460} = 11.4$ mM^{-1} cm^{-1}) are about the same as those for the wild type protein ($\varepsilon_{464} = 12.20$ mM^{-1} cm^{-1}).[6] Both variants show higher absorption around 550 nm and their spectra are red-shifted compared to XenA-wt. With coumarin (2*H*-chromen-2-one) bound to the oxidized enzyme, the absorbance maxima of XenA-wt is 470 nm. XenA-C25A with a maximum at 468 nm shows a red-shift of 2 nm, whereas the maximum of XenA-C25S is blue-shifted to 476 nm (Supplementary Data Fig. S1). The specific activities for XenA-wt and variants, measured with NADPH and 2-cyclohexenone as substrates are given in Table 1. XenA-C25A shows a sixfold decrease in specific activity, whereas the specific activity of XenA-C25S is half of XenA-wt. However, the XenA-C25A variant tended to precipitate under the assay conditions, making it likely that the low specific activity of XenA-C25A is due, at least in part, to a lower effective enzyme concentration in the assay. Furthermore, the specific activity of XenA-wt and both variants was determined at pH values ranging from 5 to 10.5 (data not shown) to detect possible changes in the pH-activity profile. The specific activities of the three XenA variants have an activity optimum around pH 8, change less than 50 % within the pH range 6 – 10 and show all the same principal pH-activity profile.

Ligand binding

XenA-wt and the two cysteine variants were titrated under identical conditions by stepwise addition of coumarin. Binding of coumarin perturbs the spectrum of XenA and therefore allows to detect complex formation (Fig. 1). Isosbestic points, consistent with a two-state binding process, are observed with all three proteins. Plots of the absorbance change at the maximum against ligand concentration and regression analysis using the Eq. (1) were used to determine the dissociation constants (K_d) for XenA-wt and the variants. K_d for the XenA-wt coumarin complex was 8.4 ($\pm$ 1.0) μM, which is similar to the value of 5.0 ($\pm$ 1.0) μM determined earlier.[6] For both variants, the exchange of cysteine resulted in small increases of the dissociation constant; a twofold increase for XenA-C25A and a sevenfold increase for XenA-C25S compared to the wild type protein (Table 1). Binding of coumarin causes no additional charge transfer interaction with strong absorbance in the long wavelength range.[19] The small changes of K_d are in agreement with a weak and likely indirect contribution of Cys25 to the formation of the complex between oxidized XenA and coumarin.

**Table 1.** Specific activities and K_d values of XenA-wt, XenA-C25A and XenA-C25S

	Specific activity (U mg^{-1})	K_d (μM) for coumarin
XenA	6.7	8.4 $\pm$ 1.0
C25A	1.11	20.9 $\pm$ 3.2
C25S	3.34	69.2 $\pm$ 3.6

Photoreduction and determination of reduction potentials

Both XenA variants were reduced using the light-mediated generation of electrons with the deazaflavin/EDTA couple in the presence of phenosafranine as redox mediator. This method was used to ensure single electron transfer and allow the formation of semiquinone species. Unlike XenA-wt, which shows the initial formation of an anionic semiquinone,[13] only quinone and hydroquinone species of FMN are observed during photoreduction of XenA-C25S and XenA-C25A (Fig. 2a). We therefore assume that, as in XenA-wt, the reduction potential of the FMN/FMNH$^-$ couple is substantially lower than the FMN/FMNH$^-$ couple and that either the enzyme or the reaction conditions allowed for faster equilibration than observed in the experiment with XenA-wt.[13] The inability to form semiquinone species has been observed also for the related flavoenzymes morphinone reductase,[20] PETN reductase[14] and YqjM.[21]

To investigate the influence of Cys25 on the relative stability of the oxidized and reduced state of XenA, we determined the reduction potentials of the FMN/FMNH$^-$ redox couple of both variants. The reduction potentials of XenA-C25A and XenA-C25S were calculated (using Eq. (4)) to be –266 mV and –181 mV, respectively. Thus, the replacement of cysteine with alanine does not change the reduction potential (XenA-wt: $E^0_m = -263$ mV),[13] whereas the exchange with serine increased the reduction potential by +82 mV. The linear fit of the plot of log(E_{ox}/E_{red}) *versus* log(Dye_{ox}/Dye_{red}) shows a slope of –1 in both cases, confirming that the enzyme and the dye received the same amount of electrons and reacted under equilibrium conditions. The determination of the reduction potential of XenA-C25A with phenosafranine as reference dye is illustrated by Fig. 2b.

The mutations of Cys25 to alanine and serine were expected to alter the reduction potential of the FMN as shown for OYE[17] and morphinone reductase.[15] The corresponding threonine residue in these two enzymes forms an O-H...O hydrogen bond to the $C_{(4)}$ oxygen atom of the isoalloxazine ring and stabilizes the negative charge of the reduced FMN. The hydrogen bond is lost when this residue is replaced by alanine and the reduction potential of the FMN/FMNH$^-$ couple is decreased from –230 mV to –263 mV in OYE[17] and from –242 mV to –290 mV in morphinone reductase.[15] As the γ-sulfhydrylgroup of Cys25 is within hydrogen bonding distance to $O_{(4)}$ of the isoalloxazine ring,
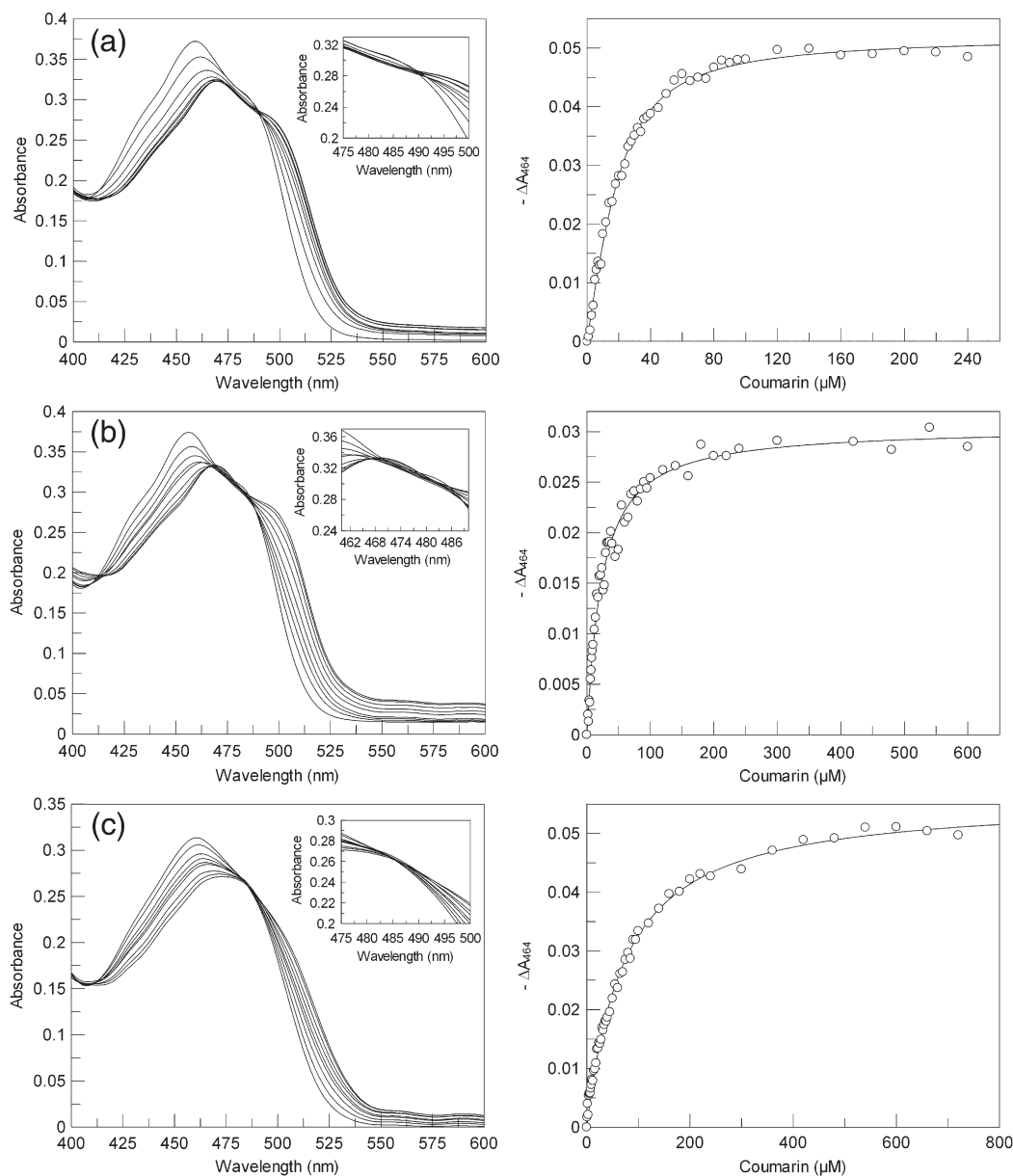
Fig. 1. Titration of XenA-wt, XenA-C25A and XenA-C25S with coumarin. Spectra were recorded in 50 mM Tris buffer, pH 8.0 at 25 °C. (a) Left-hand side: For XenA-wt (30 μM), the spectra are shown in the presence of 0, 8, 22, 38, 55, 75, 95, 160 and 200 μM coumarin. Right-hand side: A plot of absorbance changes as a function of the coumarin concentrations for the data shown on the left-hand side. (b) Left-hand side: For XenA-C25A, the spectra are shown in the presence of 0, 8, 18, 30, 45, 80, 160, 360 and 780 μM coumarin. Right-hand side: A plot of absorbance changes as a function of the coumarin concentrations for the data shown on the left-hand side. (c) Left-hand side; For XenA-C25S, the spectra are shown in the presence of 1, 10, 30, 50, 65, 85, 140, 240 and 360 μM coumarin. Right-hand side: A plot of absorbance changes as a function of the coumarin concentrations for the data shown on the left-hand side. The insets in the left-hand side of (a) – (c) show the region of the isosbestic points in detail.

we expected that the mutation to alanine would lead to a substantial decrease of the reduction potential. However, the reduction potential of XenA-C25A was practically the same as that of the wild type enzyme. This implies that either the oxidized and reduced states are equally stabile in XenA-wt and XenA-C25A or the reduced and oxidized state of the flavine are both stabilized or destabilized by the same amount upon loss of the SH group of Cys25.

The reduction potential of XenA-C25S changes to −181 mV. The difference in reduction potential of

+82 mV compared to the wild type enzyme and +87 mV compared to XenA-C25A is distinctly larger than that observed for the exchange of the corresponding threonine against alanine in OYE ($\Delta E^0_m = +33$ mV) and morphinone reductase ($\Delta E^0_m = +48$ mV). The more strongly polarized hydroxyl group of Ser25 can form a strong O-H⋯$O_{(4)}$ hydrogen bond with FMN and is therefore able to stabilize both FMN and FMNH⁻. However, the increase of reduction potentials is stronger than expected from the exchange of a weak S-H...$O_{(4)}$
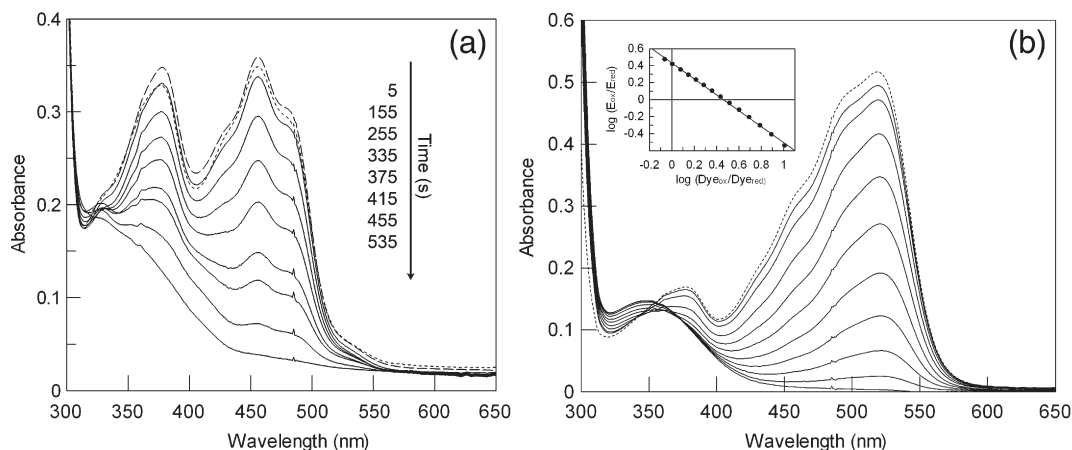
Fig. 2. Photoreduction and determination of the reduction potential of the FMN/FMNH$^-$ couple in XenA-C25A. (a) Conditions: 30 µM XenA-C25A, 15 mM EDTA, 1 µM phenosafranine, 100 mM Tris buffer, pH 8.0 and traces of 5-deaza-10-methyl-3-sulfopropyl-isoalloxazine as catalyst. The spectra are shown before (dotted line) and after different illumination steps (continuous lines). The spectrum of reoxidized XenA-C25A is displayed as a broken line. (b) Conditions: 15 µM XenA-C25A, 15 µM phenosafranine, 2 µM methylviologen, 0.05 U xanthine oxidase, 50 mM Tris buffer, pH 8.0. The reduction of XenA-C25A with phenosafranine as reference dye is shown over a time range of 1.5 h (continuous lines). The spectrum recorded before the addition of xanthine is displayed as a dotted line. Absorbance values at 456 nm and 521 nm were used to calculate the concentrations of oxidized C25A and dye. The inset shows the plot of $\log(E_{ox}/E_{red})$ against $\log(Dye_{ox}/Dye_{red})$. The continuous line displays the linear fit with a slope of –1. The reduction potential of XenA-C25A was –266 mV.

hydrogen bond by the stronger O-H...O$_{(4)}$ hydrogen bond. The small change in reduction potential upon loss of the γ-sulfhydryl group and the large change when it was exchanged for a hydroxyl group indicated that it did not form a hydrogen-bond to O$_{(4)}$.

Transient kinetic analyses of the two half-reactions

Stopped flow spectrophotometry on the two half-reactions of XenA-C25A and XenA-C25S with different substrates was used to gain further insights into the role of Cys25 for the reactivity of XenA.

To initiate the reductive half-reactions (RHR) the enzymes were mixed under anoxic conditions in the stopped flow cuvette with different concentrations of NADH and NADPH and the signal change was followed at 464 nm. The kinetics of the oxidative half-reactions (OHR) of both XenA variants were studied with various concentrations of 2-cyclohexenone and coumarin. Before the OHR, the enzymes were reduced with equimolar amounts of NADH, which was sufficient to achieve complete reduction of FMN. Both variants were mixed with 2-cyclohexenone and coumarin under anoxic conditions in the stopped flow cuvette and the signal increase was followed at 464 nm. All of the substrates were used in our earlier study of XenA-wt,[13] which allows us to compare the reactivities of the variants with that of the wild type protein.

All of the observed rate constants showed a hyperbolic dependence on the substrate concentrations used (RHR in Fig. 3a–d; OHR in Fig. 4a–d). The linear correlations between $1/k_{obs}$ and $1/$ [NADH or NADPH] (Fig. 3a–d, insets) and $1/k_{obs}$ and $1/[$2-cyclohexenone or coumarin] (Fig. 4a–d, insets) indicate equilibrium conditions for the reaction so that Eq. (7) can be used to determine the individual rate constants (k_x) and the dissociation constant (K_d) for the XenA substrate complexes.

In contrast to what was found for XenA-wt,[13] there was no indication of the formation of a charge transfer complex at 520 – 560 nm with the two variants in the RHR. The limiting rate constants of the reduction (k_{red}) of XenA-C25A were 0.76 (± 0.03) s^{-1} for the reaction with NADH and 19.0 (± 0.4) s^{-1} for the reaction with NADPH. These rate constants are slightly smaller than that found for XenA-wt and, like in the wild type enzyme, the XenA variants reacted 20-fold faster with NADPH than with NADH.[13] The limiting rate constants for the oxidation of XenA-C25A were 26.3 (± 0.1) s^{-1} with 2-cyclohexenone and 0.43 (± 0.01) s^{-1} with coumarin as substrate. The dissociation constants of all XenA-C25A substrates complexes are increased five- to sevenfold by the replacement of cysteine with alanine (RHR: NADH, 1216 (± 81) µM and NADPH, 726 (± 46) µM. OHR: 2-cyclohexenone, 346 (± 3) µM; coumarin, 109 (± 10) µM). As the reduction potentials of the FMN/FMNH$^-$ couple of XenA-C25A and XenA-wt are very similar, we expected practically unchanged rate constants for the two half-reactions. However, we observed small but consistent changes and the exchange of cysteine against alanine decreased the rate constant of the RHR by a factor of 2 and increased the rate constant of the OHR by the same factor.

The rate constants for the reduction of the XenA-C25S variant were 6.1 (± 0.2) s^{-1} for NADH and 171
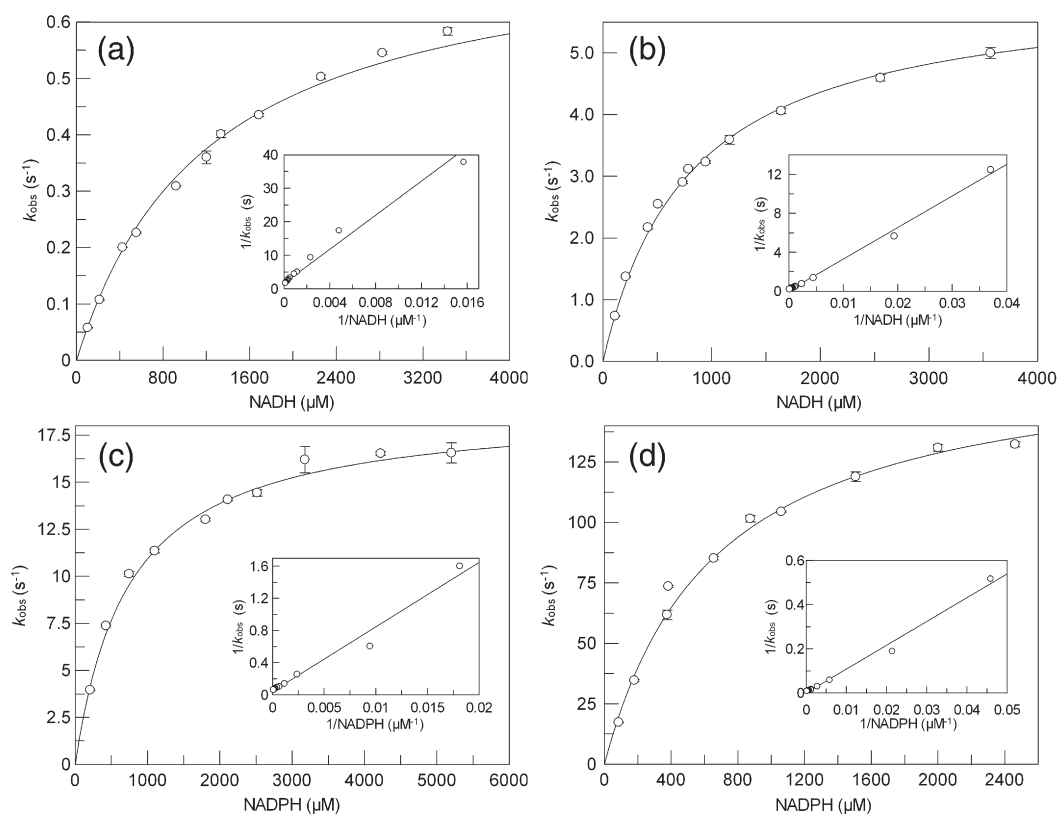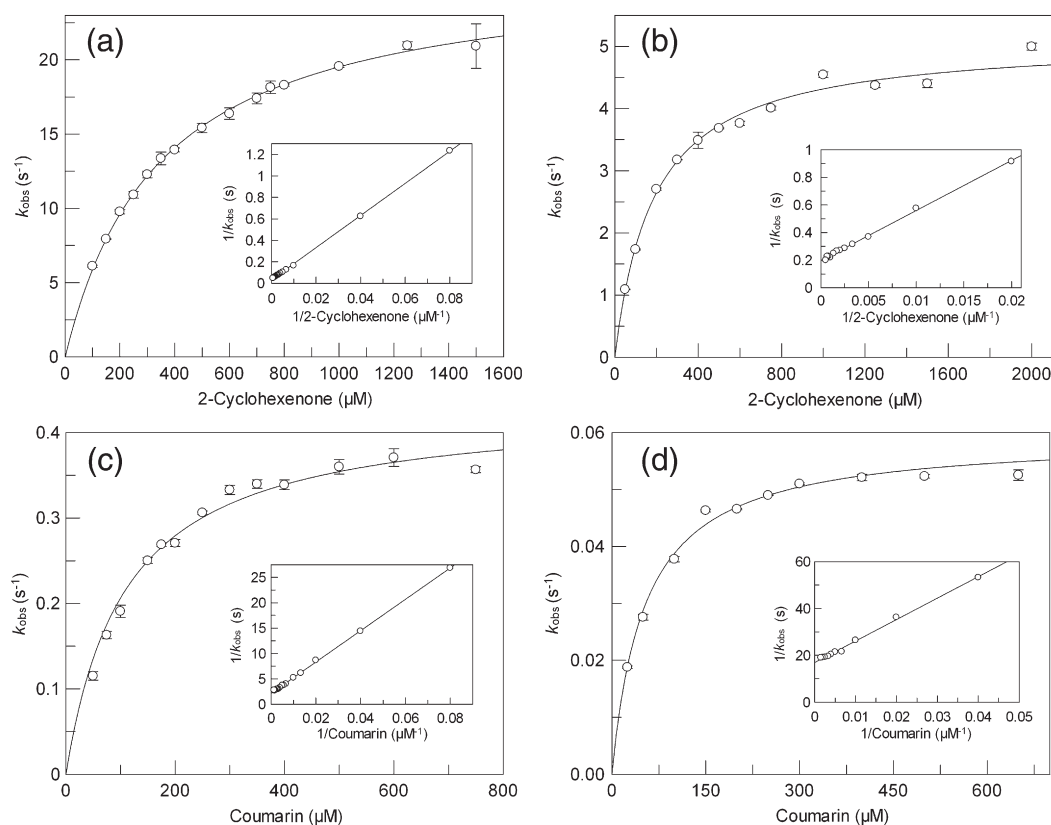
Fig. 3. Reductive half-reactions of XenA-C25A and XenA-C25S with NADH and NADPH. The concentration dependence of the observed rates at 464 nm for the reaction of 5 μM enzyme with the reductive substrates is shown. (a) Reaction of XenA-C25A with different concentrations of NADH. (b) Reaction of XenA-C25S with different concentrations of NADH. (c) Reaction of XenA-C25A with different concentrations of NADPH. (d) Reaction of XenA-C25S with different concentrations of NADPH. The reciprocal plots are shown in the insets.

($\pm$ 10) s^{-1} for NADPH, which is about three- to fourfold higher than that for XenA-wt, while the rate constants of the oxidation of XenA-C25S with 2-cyclohexenone (5.12 ($\pm$ 0.08) s^{-1}) and with coumarin (0.060 ($\pm$ 0.001) s^{-1}) are fourfold smaller than those for XenA-wt. Again, as seen with the replacement of cysteine by alanine, the rate constants of both half-reactions changed by the same factor. However, the replacement of cysteine with serine accelerated the reductive half-reaction and decelerated the oxida-tive half-reaction. The dissociation constants for all four enzyme–substrate complexes were increased. The dissociation constants of the XenA-C25S-NAD(P)H complex were 800 ($\pm$ 37) μM for NADH and 655 ($\pm$ 85) μM for NADPH, which is within the same range as that of XenA-C25A and are four- to sevenfold greater than that of XenA-wt, while the dissociation constants of the complexes with 2-cyclohexenone (187.1 ($\pm$ 7.1) μM) and coumarin (53.0 ($\pm$ 4.0) μM) were approximately doubled. The reduction potential of the FMN/FMNH^{-} couple of XenA-C25S is more positive by 82 mV than that for XenA-wt. We assume that the stronger stabilization of the reduced flavin results in product stabilization in the RHR and a destabilization of the educts in the OHR compared to the reaction of XenA-wt. A similar effect was observed for the threonine-alanine exchange in OYE and morphinone reductase.

The rate constants determined for the both half-reactions and the kinetic dissociation constants are summarized in Table 2. From these data we can conclude that Cys25 is not essential for catalysis, but its presence shifts the enzyme reactivity more to the RHR (compared to XenA-C25A) or the OHR (com-pared to XenA-C25S). Both exchanges of the cysteine residue decrease the affinity of the enzyme for its substrates corresponding to a change in the apparent binding energy ($\Delta G_{app} = RT \ln K_S / K'_S$) of 1.7 – 4.7 kJ/mol. Due to the effect of the mutations on the electronic structure and likely the conformation of the isoalloxazine ring and the $\pi\pi$ interactions of the substrate with the isoalloxazine ring, there are several different contributions to ΔG_{app}, and the local binding energy (ΔG_{bind}) between Sγ-Cys25 with the substrate may be only a small part of this sum. We therefore assume that the loss of a direct Cys25–substrate interaction, e.g. formation of a hydrogen bond in the Michaelis complexes, would have resulted in a greater increase of ΔG_{app} and we conclude that Cys25 does not contribute to the binding of the substrate in either the oxidized or the reduced state.

Active site structure of XenA-wt

The structure of XenA-wt was refined at a resolution of 1.03 Å without and at 1.1 Å with

Fig. 4. Oxidative half-reactions of XenA-C25A and XenA-C25S with 2-cyclohexenone and coumarin. All figures show the concentration dependence of the observed rates at 464 nm for the reaction of 5 μM enzyme with the oxidative substrates is shown. (a) Reaction of XenA-C25A with different concentrations of 2-cyclohexenone. (b) Reaction of XenA-C25S with different concentrations of 2-cyclohexenone. (c) Reaction of XenA-C25A with different concentrations of coumarin. (d) Reaction of XenA-C25S with different concentrations of coumarin. The reciprocal plots are shown in the insets.

coumarin bound to the active site (Fig. 5a and b). For the refinement, hydrogen atoms were included and all non-hydrogen atoms were refined with aniso-tropic *B*-factors. The high resolution revealed mul-tiple conformations for 7.5 % of the side chains. A large number of hydrogen atoms are clearly defined in the electron density, and on leaving out the amide protons of the main chain of XenA 37 % of the corresponding H atoms produce peaks with more than 0.2 e/Å^3, corresponding to a σ-level of 3.0, in the difference density map. The incomplete coverage of the observed amide hydrogens is most likely due to the correlation between the maximum electron

density peak for an atom and the root-mean-square (rms) deviation of the atomic position. To estimate whether our measuring strategy induced photore-duction of the flavin by the X-rays, we compared the bond length within the isoalloxazine ring to the values given for oxidized and reduced small flavin derivatives.[22] The FMN in XenA-wt has the follow-ing redox-sensitive bond lengths: $N_{(5)}$–$C_{(4a)}$, 1.37 Å; $C_{(4a)}$–$C_{(4)}$, 1.44 Å; $C_{(4a)}$–$C_{(10a)}$, 1.40 Å; and $C_{(10a)}$–$N_{(1)}$, 1.31 Å. These values are not typical for oxidized or reduced flavins and are intermediate between the distances expected for both oxidation states. These deviations might reflect the influence of the protein

Table 2. Transient kinetic data

	XenA-wt[a]		XenA-C25A		XenA-C25S	
	k_{red} (s^{-1})	K_d (μM^{-1})	k_{red} (s^{-1})	K_d (μM^{-1})	k_{red} (s^{-1})	K_d (μM^{-1})
NADH	1.50±0.02	176±14	0.76±0.03	1216±81	6.1±0.2	800±37
NADPH	35.7±0.6	256±12	19.0±0.4	736±47	171±11	656±86
	k_{ox} (s^{-1})	K_d (μM^{-1})	k_{ox} (s^{-1})	K_d (μM^{-1})	k_{ox} (s^{-1})	K_d (μM^{-1})
2-Cyclohexenone	13.1±0.1	86±2	26.3±0.1	346±3	5.12±0.08	187±7
Coumarin	0.243±0.001	19.3±0.6	0.43±0.01	109±10	0.060±0.001	53±4

[a] Data from the wild type enzyme XenA are from Ref. [12].
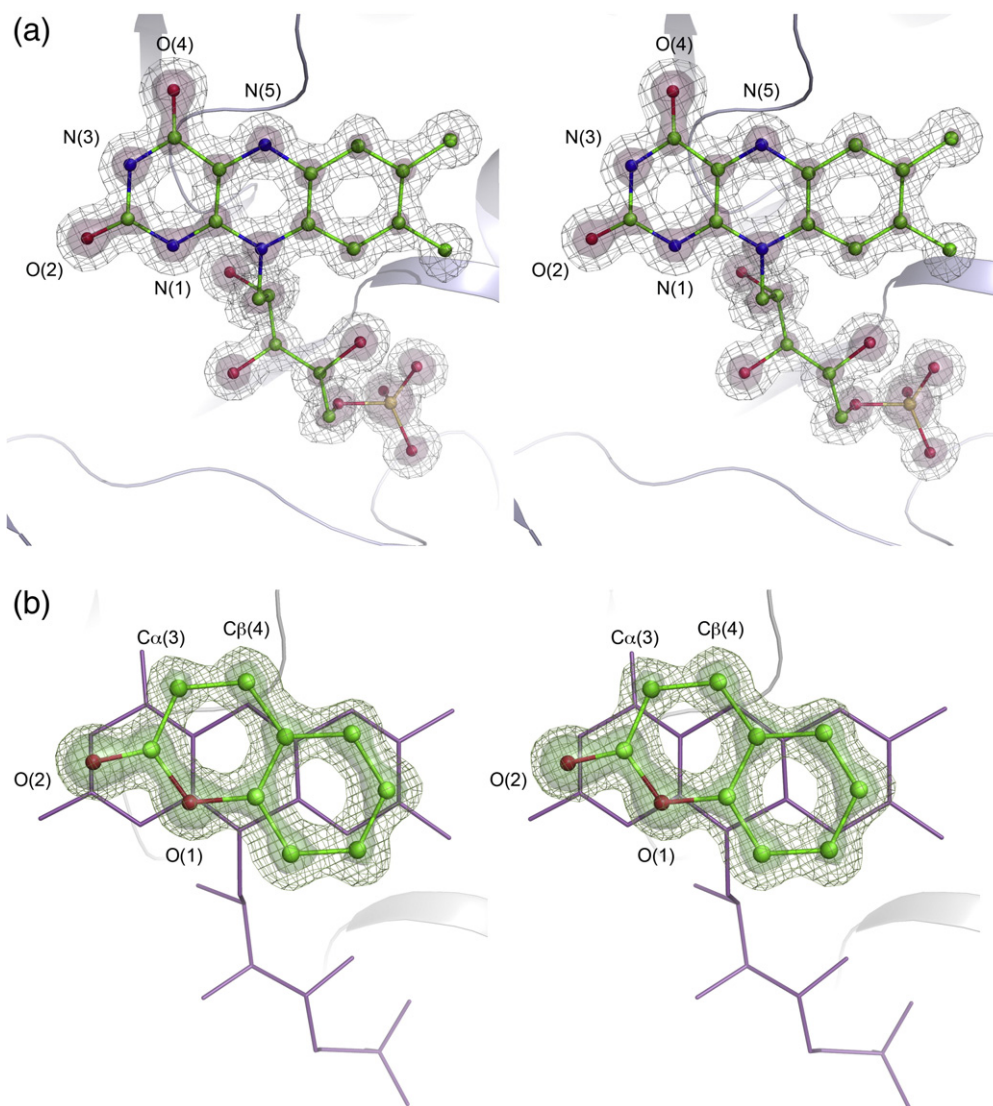
Fig. 5. Atomic resolution structure of XenA-wt. (a) Stereoscopic view of the electron density map of the FMN cofactor. The $2F_o - F_c$ map contoured at 1.0σ is shown in gray mesh representation, the $2F_o - F_c$ map contoured at 5.0σ is shown in brown surface representation. FMN is shown in stick and ball mode. Oxygen atoms, red; nitrogen atoms, blue; carbon atoms, green; and phosphorus, yellow. (b) Stereoscopic view of FMN in complex with coumarin. The $2F_o - F_c$ map contoured at 1.0σ is shown in green mesh representation and the $2F_o - F_c$ map contoured at 5.0σ is shown in green surface representation. FMN (violet) is shown in stick mode. Coumarin is displayed in stick and ball representation with carbon atoms in green and oxygen atoms in red.

environment on the geometry of the cofactor. However, it is likely that the synchrotron radiation, at least in part, reduced the protein during data collection resulting in a mixture of oxidized and reduced molecules. We therefore refrain from an in-depth discussion of the flavin geometry. Nevertheless, the improvement in resolution provides a better description of the active site structure, particularly on the protein–cofactor and protein–substrate inter-actions. The atomic resolution structure allows us to reassess the geometry of residues with an unusual conformation. In the earlier structure, a single tryptophan residue (Trp358) was found to deviate from the Ramachandran statistics. This deviation is likely of functional relevance, as Trp358 is part of the FMN-binding site and the unusual conformation of

the peptide backbone has been confirmed in the atomic resolution structure.

Furthermore, the electron density can provide direct insight in the charge distribution throughout the isoalloxazine ring, provided the ring atoms have comparable B-factors. The average B-factor of the ring atoms was 6.0 Å^2, and the deviations from this value were within $\pm 15\%$. The electron density distribution was lowest within the dimethylbenzene ring and stronger for the heteroaromatic rings. These areas are expected to interact favorably with donor atoms.[23,24] The FMN cofactor is non-covalently bound to the protein by different interactions between the protein environment and the FMN. Hydrogen bonding interactions are located exclusively in the area of higher charge density (Fig. 6a). $O_{(4)}$ of the isoalloxa-
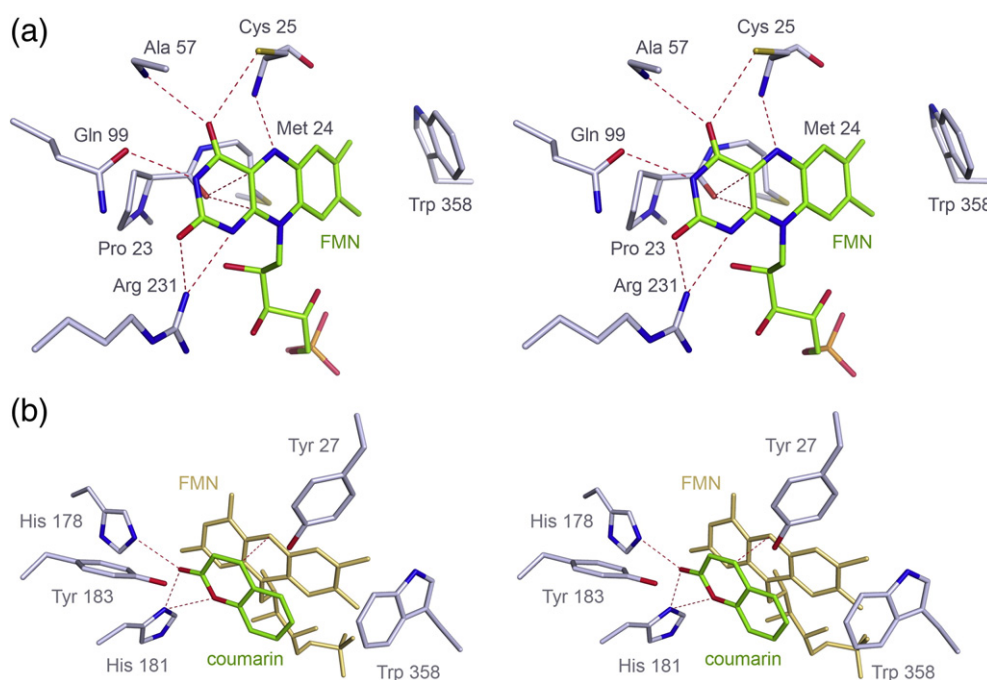
Fig. 6. Active site view. (a) Stereoscopic view of the hydrogen-bonding network around FMN. All residues are displayed in stick representation. Carbon atoms of the amino acid side chains, gray; carbon atoms of FMN, green; oxygen atoms, red; nitrogen atoms, blue, sulfur atoms, yellow; and phosphorus, orange. The broken red lines represent possible interactions between the cofactor and the adjacent amino acids. (b) Stereoscopic view of the hydrogen bonding network around coumarin bound to the active site. All residues are displayed in stick representation. FMN, yellow; carbon atoms of coumarin, green; carbon atoms of the amino acid side chains, gray; oxygen atoms, red; and nitrogen atoms, blue. The broken red lines represent possible interactions between coumarin and XenA-wt.

zine ring is within hydrogen bonding distance to the amide proton of Ala57 and the γ-sulfhydryl group of Cys25. The distance between the γ-sulfhydryl group of Cys25 and $O_{(4)}$ is 3.28 Å, indicating that a weak hydrogen bond might be present. $N_{(5)}$ is within hydrogen bonding distance to the amide proton of Cys25. $N_{(1)}$ as well as $O_{(2)}$ are within hydrogen bonding distance to the guanidinium group of Arg231 with a distance of 2.99 Å and the proton of $N_{(3)}$ interacts with the carbonyl group of Gln99 with a N–O distance of 2.80 Å.

The dimethylbenzene ring is stabilized by a face-on-edge π–π interaction with Trp358 of the second monomer and hydrophobic interactions with Met24 on the *re* side. Further close contacts between protein and cofactor are found for the $C_{(4a)}$ and $C_{(10a)}$ atoms of the isoalloxazine ring, which are only 3.06 Å away from the carbonyl oxygen of Pro23. The oxygen atom is positioned exactly in the middle below the bond between $C_{(4a)}$ and $C_{(10a)}$ on the *re* side and it is substantially closer to the two carbon atoms than the van der Waals radii would suggest. The isoalloxazine ring is distinctly non-planar. This deviation from planarity might be, in part, a consequence of a partial photoreduction of the ring. However, given the short distance between Cys25 Sγ and $O_{(4)}$ and the observed non-planarity of the flavin of crystals exposed to a lose dose of radiation,[6] it appears to be unlikely that the isoalloxazine ring is planar in the oxidized state, as that would lead to a strong overlap of the van der Waals radii of the two atoms if Cys25 is kept fixed.

The observed overlap of the van der Waals radii between the carbonyl oxygen of Pro23 and the $C_{(4a)}$ and $C_{(10a)}$ carbon on the *re* side of the flavin with the short S...$O_{(4)}$ distance in the *si* side indicated that the protein environment exerts a considerable strain on the isoalloxazine ring and that Cys25 is part of a protein clamp for the cofactor. The active site pocket is not empty and a sulfate molecule, a constituent of the crystallization solution, is bound above the *si* side of the isoalloxazine ring.

Active site structure with bound coumarin

The crystal structure of true Michaelis complexes between enzyme and substrates are difficult to achieve due to their inherent reactivity. As a substitute, we determined the structure of oxidized XenA in complex with coumarin to infer the relative orientation of substrate and cofactor. The structure of XenA-wt with coumarin bound was refined at a resolution of 1.10 Å (Fig. 6b). The statistics of the dataset revealed that the overall quality is not as good as that of the other datasets and we believe the lower data quality is the reason why the *R* value for the model is not as low as expected for a structure at this resolution (Table 4). There is no indication of structural change occurring upon coumarin binding, and the Cα atoms of the substrate-bound and substrate-free structures can be superimposed with an rms deviation of 0.09 Å. Coumarin is bound nearly coplanar above the isoalloxazine ring,
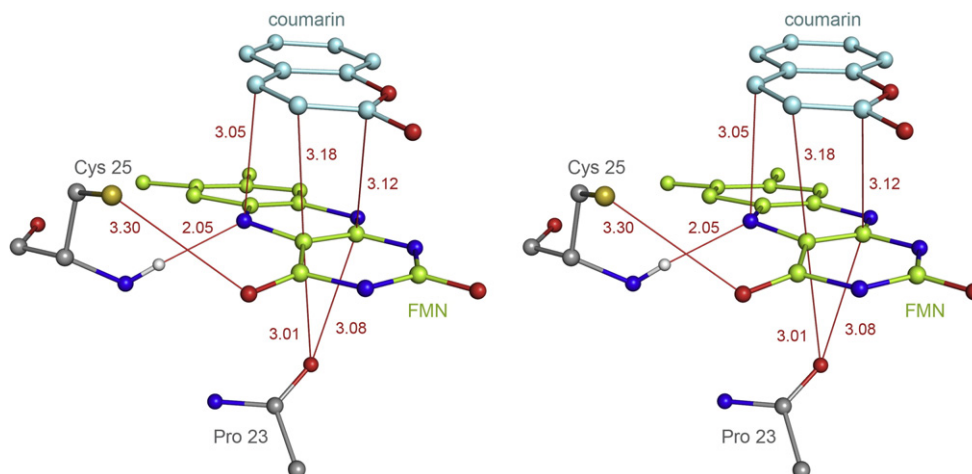
Fig. 7. Compression of the flavin in the coumarin complex. Stereoscopic view of the active site of XenA-wt in complex with coumarin. All residues are shown in stick and ball representation. Carbon atoms of the amino acid side chains, gray; carbon atoms of FMN, green; carbon atoms of coumarin, light blue; oxygen atoms, red; nitrogen atoms, blue; sulfur atoms, yellow; and hydrogen atoms, white. Distances between atoms are given (in ångström units) and are displayed as red lines.

consistent with π–π interactions between both molecules (Fig. 6b). The carbonyl oxygen of coumarin is within hydrogen bonding distance to His178 (2.90 Å) and His181 (2.84 Å). His181 is also in hydrogen bonding distance to $O_{(1)}$ of coumarin. The closest contact between coumarin and the isoalloxazine ring is between the β carbon of coumarin and $N_{(5)}$ of FMN. The distance of 3.05 Å is shorter than expected from the van der Waals radii (van der Waals distance 3.2 Å), indicating that the enamine moiety of FMN is sterically compressed from both sides in the substrate-bound form (Fig. 7). While the carbonyl oxygen of Pro23 is close to $C_{(4a)}$ and $C_{(10a)}$ on the *re* side of the flavin, coumarin presses on the *si* side of the isoalloxazine ring. The short distance between $N_{(5)}$ and the β carbon of coumarin is especially notable, as the observed compression could facilitate the electron/hydride transfer between the atoms. A role of sterical compression to enhance catalysis has been suggested.[25–27] The α carbon of coumarin is 3.28 Å away from the potential catalytic proton donor Tyr183 (Fig. 6b). The shortest distance between the γ-sulfhydryl group of Cys25 and the coumarin ring is 4.0 Å and there is no indication of a direct interaction between coumarin and Cys25, nor does the conformation of Cys25 change upon coumarin binding. The principal arrangement of the enzyme-bound flavin and the substrate is similar to the average geometry found in a number of flavoenzymes,[28] in which the carbon atom of the substrate to be activated by electron/hydride transfer from the $N_{(5)}$ atom is, on average, 3.5 Å away (here 3.05 Å) and makes an angle with the $N_{(5)}$-$N_{(10)}$ atoms of 96–117° (here 98°).

Structures of XenA-C25A and XenA-C25S alone and in complex with coumarin

The structures of XenA-C25A and XenA-C25S were solved at resolutions of 1.20 Å and 1.80 Å,

respectively (Fig. 8a and b). The overall structures of both mutant enzymes reveal no significant changes of the protein conformation and confirm the exchange of Cys25 with Ser and Ala. All other residues in the active site are unaltered and superimpose exactly with the structure of XenA-wt. The replacement of cysteine by serine brings a stronger hydrogen bond donor/acceptor into the active site, while the replacement of cysteine by alanine creates a small void and both can perturb the local water structure. The high resolution of the two variants clearly defines the location of individual ordered water molecules, which are superimposable with XenA-wt in both cases, indicating that the mutations have no effect on the water structure of the active site.

The atomic resolution structures of XenA-wt and XenA-C25A provide a better description of the bending of the isoalloxazine ring (Fig. 9a). In comparison to the subatomic resolution structure of PETN reductase[10] and the 1.3 Å resolution structure of YqjM,[12] the isoalloxazine rings of XenA-wt and XenA-C25A are more domed and point with the ends towards its *re* side. Furthermore, the $C_{(4)}$–$O_{(4)}$ carbonyl group of the pyrimidine rings is moved further out of the ring plane towards the *re* side of the FMN (Fig. 9b). XenA-C25S did not show these distortions. Here, the isoalloxazine as well as the pyrimidine ring are more planar, allowing the hydroxyl group of serine and $O_{(4)}$ of FMN to be within the typical hydrogen bond distance of 2.8 Å. However, the structures of the C25S variant have been determined at lower resolution and the interpretations of the distortion of the isoalloxazine-ring are less reliable. The position of coumarin in the active site pocket (Fig. 8c and d), as well as the interactions between protein and coumarin, are indistinguishable for XenA-wt, XenA-C25A and XenA-C25S (Fig. 9b).

The structures of the two XenA variants show that the effects of the cysteine exchanges are only local
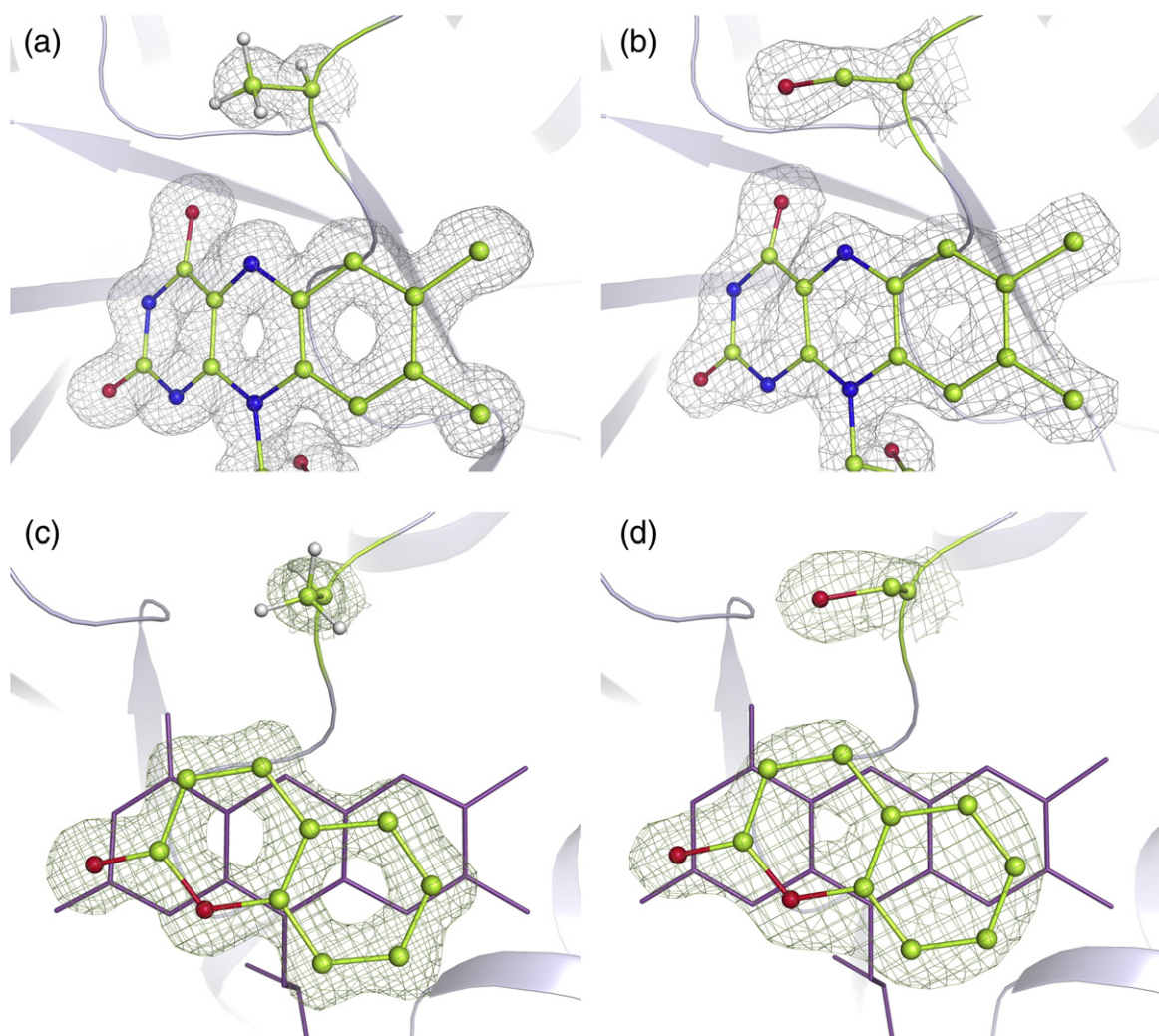
Fig. 8. XenA variants. (a) Active site of XenA-C25A. The $2F_o - F_c$ map contoured at 1.0σ is shown in gray mesh representation. (b) Active site of XenA-C25S. The $2F_o - F_c$ map contoured at 1.5σ is shown in gray mesh representation. All residues are displayed in stick and ball mode. Carbon atoms, green; nitrogen atoms, blue; oxygen atoms, red; and hydrogen atoms, white. (c) Active site of XenA-C25A in complex with coumarin. The $2F_o - F_c$ map of coumarin and Ala25 contoured at 1.5σ is shown in green mesh representation. (d) Active site of XenA-C25S in complex with coumarin. The $2F_o - F_c$ map of coumarin and Ser25 contoured at 1.5σ is shown in green mesh representation. FMN (violet) is displayed in stick mode. Coumarin and residues 25 are displayed in stick and ball mode. Carbon atoms, green; oxygen atoms, red; and hydrogen atoms, white.

and do not result in any further change of the active site. The conserved position of the substrate confirms that Cys25 is not important for the placement of the substrate in the active site, nor does it change the conformation of residues relevant for substrate binding. We can thus be confident that the observed changes of the spectra, reduction potential and reactivity of XenA, originate from the exchange of the γ-sulfhydryl group of Cys25 and not from further structural perturbations, which are frequently caused by mutations.

Conclusions

Its central place within the active site just above the $N_{(5)}$ atom of the isoalloxazine ring (Fig. 6a) suggested that Cys25 could be involved in the

interaction with and conversion of the substrates. To understand how Cys25 contributes to fine-tune the chemistry of the flavin cofactor, we investigated its role in the structure, reduction potential, substrate binding and reactivity of XenA.

The γ-sulfhydryl group of Cys25 is close to the bound substrate in the crystal structure of oxidized XenA (Fig. 6b) and only small rearrangements within the active site would be necessary for a direct interaction. As we have no direct insight into the structure of the true Michaelis complex, we determined the dissociation constants of the substrate – XenA variant complexes and compared it to XenA-wt. Both Cys25 variants of XenA have a slightly decreased affinity for the substrates, which argues that Cys25 contributes to substrate binding. However, changes of two to sevenfold in the dissociation constants are less than expected for the loss of a
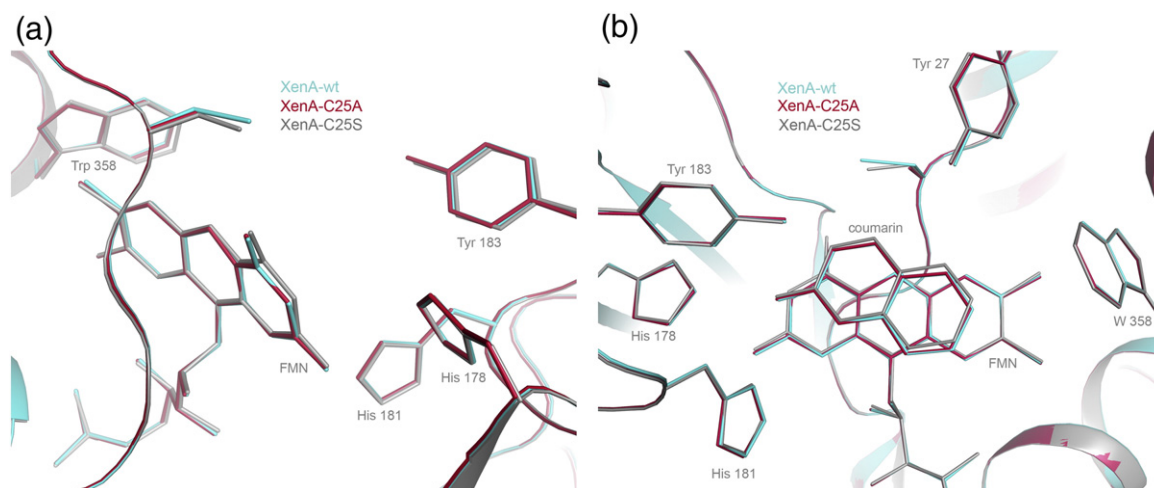
Fig. 9. Comparisons. (a) View of the active site of the superimposition of XenA-wt (blue), XenA-C25A (red) and C25S (grey). (b) View of coumarin bound to the active site of the superimposition of: XenA-wt, blue; XenA-C25A, red; and C25S, gray. All residues are shown in stick mode.

direct interaction between enzyme and substrate and are in agreement with an indirect role of Cys25 in substrate binding. This indirect role could be the modulation of the electronic structure of the isoalloxazine ring by restraining its planarity, which is in agreement with the short distances found in the active site (Fig. 7) and the bent conformation of the isoalloxazine ring.

In the structure of YqjM, Cys26 was shown to have two conformations in the absence of bound ligands: in one conformation the γ-sulfhydryl group is closer to $O_{(4)}$ and in one it is within hydrogen bonding distance to $N_{(5)}$.[12] The conformational change was not dependent on the oxidation state of YqjM and the modeled structures of oxidized and reduced YqjM are virtually identical.[12] To determine whether a conformational change of Cys25 contributes to the reactivity of XenA, we compared the reactivity of XenA-wt with XenA-C25A. The C25A variant is only twofold slower in the RHR and twofold faster in the OHR than XenA-wt, indicating that if there is a conformational change of Cys25 during the reaction, it does not contribute to catalysis and even the loss of the γ-sulfhydryl group does not compromise the reactivity of XenA.

Cysteine residues typically have pK_a values around 8.3[29] and can act as catalytic acids. As the γ-sulfhydryl group of Cys25 is close to the $Cβ = Cγ$ double bond of coumarin to which in the course of the reaction two protons and two electrons are transferred, we speculated that Cys25 might act as proton donor in the reaction. However, our analysis showed that: (I) the activity of XenA varies weakly with pH and the same profile is observed for XenA-wt, XenA-C25A and XenA-C25S; (II.) the loss of activity upon replacing Cys25 with alanine is modest in both half reactions; and (III.) the calculated protonation probability reveals it to be protonated over a wide pH range. We therefore conclude that Cys25 does not act as a proton donor in the reaction and it is most likely protonated during the complete course of the reaction.

On the basis of our experiments, we conclude that Cys25 is not essential for the reactivity, but modulates substrate binding and the reduction potential of XenA. Modulation of the reduction potential is of physiological relevance in this class of enzymes. While it is likely that in the reductive half-reaction reduced nicotinamide is used as a substrate, a wide range of substrates might be converted in the oxidative half-reaction. Depending on the substrates, either the oxidative or the reductive half-reaction can become rate limiting. We used Eq. (8), which is valid for ping pong mechanisms, to calculate the influence of each individual rate constant on the turnover number (k_{cat}) under substrate-saturated conditions. With coumarin as a substrate, the limiting reaction is always the OHR and thus the highest turnover can be achieved by XenA-C25A. With 2-cyclohexenone as substrate, either the OHR or the RHR can be rate limiting, depending on the XenA variant and the substrate in the RHR. While the RHR is rate limiting for XenA-wt and XenA-C25A with NADH as reducing substrate, the rate of both half-reactions are balanced in XenA-C25S and, indeed, XenA-C25S can achieve the highest turnover for this substrate. With NADPH as reducing substrate, both XenA-wt and XenA-C25A have a high turnover under which none of the two half-reactions is limiting, while XenA-C25S is severely limited by a slow OHR and has a lower turnover number than the other variants.

Several copies of sequences homologous to XenA are found in the genome of *P. putida*[4] and three of the copies have a cysteine residue, two have a threonine residue and one has an alanine residue in place of Cys25. A common characteristic for many enzymes of the OYE family is a wide range of possible substrates in the OHR. It is tempting to speculate that the different active site residues at the position of Cys25 in XenA adapt the enzymes for different classes of substrates, such that none of the two half-reactions severely limits

the rate of the overall reaction. This would be a further indication that the different xenobiotic reductases in *P. putida* could participate in the several pathways along which aromatic/heteroaromatic substrates are degraded and helps us to understand how such a wide range of substrates can be converted by a single microorganism.[30]

Materials and Methods

Chemicals and enzymes

All materials were purchased from Fluka, AppliChem, Roth and Otto Nordwald. Microbial media were prepared as described.[31] 5-Deaza-10-methyl-3-sulfopropyl-isoalloxazine was a gift from Peter M.H. Kroneck (University of Konstanz, Germany).

Mutagenesis, protein expression and purification

The mutation of Cys25 was done with the QuickChange mutagenesis protocol from Stratagene. The PCR primers were: for C25A

5′-GCCATTCCGCCGA-TG*G*CCCAATACATGGCC-GAAG-3′
5′-CTTCGGCCATGTATTG*GG*CCATACA-TGGC-CGAAG-3′

and for C25S

5′-GCCATTCCGCCGATG*A*GCCAATACATGGCC-GAA-GAC-3′
5′-GTCTTCGGCCATGTATTG*GCT*CATCGGCG-GAATGGC-3′

pET_XenA was used as the template as described.[6] The double-stranded wild type DNA was removed by digestion with the restriction enzyme DpnI. The mutated genes *xenA*_C25A and *xenA*_C25S were sequenced by Eurofins MWG Operon. The mutated plasmids were transformed into the expression strain *Escherichia coli* Rosetta(DE3)pLysS and the genes were expressed as the wild type gene *xenA*.[6,13] Both enzyme variants XenA-C25A and XenA-C25S were purified as described for XenA-wt, including a reconstitution with FMN before the final size-exclusion chromatography step.[6,13] The yield from 4 L of cell culture was 190 mg of the XenA-C25A variant and 180 mg of the XenA-C25S variant, both with purity exceeding 95% as estimated by SDS-PAGE (data not shown). Activity assays were done in 50 mM Tris buffer (pH 8.0), 150 μM NADPH, 300 μM 2-cyclohexenone at 25 °C. The reaction mixture was flushed with nitrogen gas in a quartz cuvette sealed by a screw-cap with a rubber septum. The reaction was started by using a Hamilton syringe to add 5 μL of the enzymes (2 mg mL^{-1}) to 995 μL of reaction buffer. The signal was followed for 2 min at a wavelength of 340 nm. One activity unit (U) is defined as the oxidation of 1 μmol of NADPH per minute. Flavin contents were determined by treatment with SDS as described.[32] Extinction coefficients of protein-bound FMN were calculated for both variants, for which the protein was denatured by the addition of 0.05 volume of 10% (w/v) SDS. After incubation for 10 min at room temperature, a spectrum was recorded to follow the release of FMN from the protein. The extinction coefficient of the enzyme-bound flavin was calculated from the known extinction coefficient of free FMN (12.200 M^{-1} cm^{-1}).

Ligand binding studies

Oxidized XenA (XenA-wt, XenA-C25A, XenA-C25S) at a concentration of 30 μM in 50 mM Tris buffer (pH 8.0) in a 1 cm quartz cuvette at 25 °C was titrated by addition of small amounts of a coumarin stock solution. Absorption spectra from 200 nm to 800 nm were recorded using an Agilent 8453 UV-visible spectrophotometer. Changes of absorption at 464 nm were plotted against ligand concentration. Dissociation constants (K_d) for the enzyme–ligand complex were determined by non-linear regression analysis of the data with GraFit-5 (Version 5.0, Erithacus Software Limited, UK) using:

$$\Delta A = \frac{\Delta A_{\max}}{2nE}\left[(L + nE + K_d) - \left((L + nE + K_d)^2 - (4LnE)\right)^{0.5}\right] \quad (1)$$

where $\Delta A_{\max}$ is the maximum absorbance change at 464 nm, L is the total ligand concentration, E is the total enzyme concentration and n is the number of ligand-binding sites.

Photoreduction and determination of reduction potentials

Photoreduction of XenA variants was done in a glass tonometer with a cuvette side arm as described.[33] We used the potassium salt of 5-deaza-10-methyl-3-sulfopropyl-isoalloxazine as the photoreductant in catalytic amounts. The reaction mixture contained final concentrations of 15 mM EDTA, 30 μM enzyme and 1 μM phenosafranine as electron mediator in 100 mM Tris buffer (pH 8.0) and was made anoxic by repeated evacuation and flushing with nitrogen gas. Solutions of the deazaflavin derivative and EDTA were stored in the side arm cuvette during this process and mixed with the enzyme directly before the light irradiation steps were performed with a 100 W lamp from a slide projector (Agfa, Opticus 100). Each illumination step lasted 10 s and absorption spectra were recorded for 3 min after the illumination. To check for reversibility of the reduction, air was allowed to enter the tonometer and cuvette after the photoreduction of the enzyme was complete and a UV/vis spectrum of the reoxidized sample was recorded. The determination of the reduction potential was done as described.[34] We used phenosafranine ($E^0_{m,D} = -252$ mV[35]) with XenA-C25A and anthraquinone-2,6-disulfonate ($E^0_{m,D} = -184$ mV[36]) with XenA-C25S as reference dyes. The absorbance values and corresponding extinction coefficients used to calculate the concentrations of oxidized enzyme and dye are given in Table 3. Concentrations of oxidized enzyme (E_{ox}) and oxidized dye (Dye_{ox}) were calculated with Eqs (2) and (3).

$$A^{456} = \varepsilon_{456}^{Eox}c^{Eox} + \varepsilon_{456}^{Dox}c^{Dox} + \varepsilon_{456}^{Ered}\left(c^{Etot} - c^{Eox}\right) + \varepsilon_{456}^{Dred}\left(c^{Dtot} - c^{Dox}\right) \quad (2)$$

$$A^{521} = \varepsilon_{521}^{Eox}c^{Eox} + \varepsilon_{521}^{Dox} + c^{Dox} + \varepsilon_{521}^{Ered}\left(c^{Etot} - c^{Eox}\right) + \varepsilon_{521}^{Dred}\left(c^{Dtot} - c^{Dox}\right) \quad (3)$$

Table 3. Absorbance values and molar extinction coefficients

	Absorbance value (nm)	Molar extinction coefficient (M^{-1} cm^{-1}) oxidized form	Molar extinction coefficient (M^{-1} cm^{-1}) reduced form
C25A	456	12.7×10^3	0.6×10^3
	521	2.1×10^3	0.6×10^3
Phenosafranine	456	11.2×10^3	0.3×10^3
	521	44.7×10^3	0.3×10^3
C25S	460	11.4×10^3	0.5×10^3
	328	4.7×10^3	4.7×10^3
Anthraquinone-2, 6-disulfonate	460	0	1.2×10^3
	328	5.7×10^3	0

Equations (2) and (3) are displayed for XenA-C25A and the reference dye phenosafranine. For XenA-C25S and the reference dye anthraquinone-2,6-disulfonate, the listed (Table 3) absorbance values and corresponding molar extinction coefficients were used respectively. The reduction potential of XenA ($E^0_{m,E}$) was determined from the difference (ΔE^0) in the reduction potentials of enzyme and dye (see Eq. (4)).

$$E^0_{m,E} = E^0_{m,D} + \Delta E \qquad (4)$$

Stopped-flow spectrophotometry

Reductive half-reaction

The reductive half reactions of the mutant enzymes with NADH and NADPH were measured in 50 mM Tris buffer (pH 8.0) under anoxic conditions at 20 °C as described.[13] The reactions were monitored at 464 nm with an Applied Photophysics SX-20MV kinetic spectrophotometer with a 1 cm observation pathlength cuvette. Enzyme at a concentration of 10 μM was mixed with NAD(P)H at concentrations of 50 – 11,000 μM. The measurement was done at least five times for each concentration of substrate.

Oxidative half-reaction

2-Cyclohexenone and coumarin were used as oxidative substrates with concentrations of 50 – 5000 μM. To achieve complete reduction the enzymes were reduced by titration with appropriate amounts of NADH in a glass tonometer with a cuvette side arm. The observed kinetic transients at 464 nm for reductive and oxidative half-reactions were fit to single-exponential equations using Pro-Data software (Applied Photophysics, UK). The rate constants (k_{obs}) were plotted against the respective substrate concentrations. The reductive half-reaction was modeled as:

$$A + B \overset{K_d}{\rightleftharpoons} C \overset{K_{red}}{\rightarrow} D \qquad (5)$$

where A is the enzyme in the oxidized state, B is the reductive substrate – NAD(P)H, C is the enzyme$_{ox}$ – substrate charge-transfer complex and D is the enzyme containing the two-electron reduced state of FMN and bound NAD(P)$^+$. The oxidative half-reaction was modeled as:

$$E + F \overset{K_d}{\rightleftharpoons} G \overset{K_{ox}}{\rightarrow} H \qquad (6)$$

where E is the enzyme in the reduced state, F is the oxidative substrate – 2-cyclohexenone, coumarin, G is the enzyme$_{red}$ – substrate charge-transfer complex and H is the oxidized enzyme with bound product (2-cyclohexanon, chroman-2-one).

The hyperbolic plots were fit to Eq. (7) using the program GraFit-5 (Version 5.0, Erithacus Software Limited, UK) to obtain the limit of the reaction rate $k_{red/ox}$ at high substrate concentrations [S] and the dissociation constant K_d:[37]

$$k_{obs} = k_X[S] / (K_d + [S]) \qquad (7)$$

Equation (8) was used to relate the limiting rate constants to the steady-state catalytic constants:

$$k_{cat} = \frac{k_{red}k_{ox}}{(k_{red} + k_{ox})} \qquad (8)$$

Calculation of protonation probabilities

The protonation of Cys25 and all other titratable residues in the protein were calculated using a continuum electrostatic approach combined with a Monte Carlo (MC) titration.[38,39] The Poisson–Boltzmann equation was solved by a finite-difference method using the MEAD program suite.[40] All aspartate, histidine, glutamate, lysine, arginine, and tyrosine residues were considered as protonatable sites. Atomic partial charges for standard amino acid groups were taken from the CHARMM27 parameter set.[41] The pK_a values of the model compounds were taken from the literature.[39,42] The partial charges of FMN were obtained by fitting the electrostatic potentials derived from density functional calculations using ADF.[43] The dielectric constant of the protein was set to 4, and that of the solvent was set to 80. The ionic strength was set to 0.1 M. The thickness of the ion exclusion layer was set to 2.0 Å. Continuum electrostatics calculations were performed using the focusing technique[44] in two steps using a grid with 151^3 points. The outer grid had a grid spacing of 1.0 Å and was placed at the geometric center of the protein. The inner grid had a grid spacing of 0.25 Å and was centered at the titratable site. A similar procedure was used for the model compound, with all grids centered at the titratable site.

The protonation probabilities were calculated for pH values of 0 to 14 in steps of 0.2 using Metropolis MC. The temperature was set to 300 K. At each pH value, a randomly chosen initial state vector was equilibrated with 200 MC scans, where one MC scan comprises as many MC moves as there are titratable sites in the protein. Subsequently, 10,000 MC scans were performed to determine the protonation probability of each site.

Data collection and structure refinement

Crystals of the XenA mutants were grown as described for the wild type XenA.[6] The crystals were cross-linked for 1 h in a harvesting solution containing 100 mM Hepes (pH 7.5), 2.4 M ammonium sulfate and 0.002% (v/v) glutaraldehyde. To soak crystals with substrate, they were further incubated for 1 h in harvesting buffer containing approximately 5 mM coumarin. Crystals were shock-frozen in harvesting buffer containing 20% (v/v) 2R,3R-butanediol and stored in liquid nitrogen. The crystals belong to the space group *I*222 and the cell dimensions are given in Table 4. X-ray

Table 4. Crystallographic data and refinement statistics

	XenA-wt		XenA-C25A		XenA-C25S	
	Native	Coumarin	Native	Coumarin	Native	Coumarin
A. *Data collection*						
Spacegroup cell constants a (Å)	*I222*	*I222*	*I222*	*I222*	*I222*	*I222*
a (Å)	57.89	57.99	58.06	57.77	57.99	58.33
b (Å)	83.41	83.37	83.27	83.62	83.61	83.56
c (Å)	156.72	156.67	157.63	157.17	157.24	156.72
Wavelength (Å)	0.9184	0.9184	0.9184	0.9184	0.9184	0.9184
Total reflections	750,322	555,063	405,950	338,576	125,475	129,228
Unique reflections	180,933	147,817	110,585	96,594	64,188	36,914
Resolution (Å)	30-1.02	30-1.10	30-1.20	30-1.28	30-1.80	30-1.75
	(1.06–1.03)	(1.13–1.10)	(1.23–1.20)	(1.31–1.28)	(1.85–1.80)	(1.80–1.75)
R_s[a] (%)	5.7 (58.7)	9.3 (43.0)	4.9 (46.7)	6.2 (54.9)	4.7 (31.4)	6.5 (44.8)
Completeness (%)	97.1 (86.8)	96.4 (94.8)	92.8 (86.4)	98.5 (88.2)	93.7 (80.1)	94.5 (83.3)
$I / \sigma I$	13.11 (2.16)	8.82 (2.54)	14.22 (2.76)	12.75 (2.31)	12.54 (2.26)	14.05 (2.64)
B. *Refinement*						
R_{work} / R_{free} (%) [b]	12.9 / 14.8	19.0 / 21.6	12.5 / 14.9	13.4 / 16.4	18.2 / 23.0	18.0 / 21.2
rms deviation from ideality						
Bond length (Å)	0.010	0.012	0.011	0.011	0.006	0.006
Bond angle (°)	1.42	1.47	1.39	1.41	0.96	0.98
No. molecules						
Atoms/ASU [c]	3600	3565	3623	3689	3445	3469
Ligand/ion	10	12	10	11	9	11
Water	587	561	143	622	599	596
Estimated coordinate errors based on						
R	0.021	0.039	0.034	0.044	0.147	0.131
R_{free}	0.023	0.039	0.034	0.042	0.141	0.122

Values in parentheses are for the highest resolution shell.

The Friedel mates of the native data set of XenA-C25S were treated as independent reflections to allow the use of the anomalous scattering to detect the presence/absence of sulfur.

[a] $R_s = \Sigma_h \Sigma_i \mid I_i(h) - <I(h)> \mid / \Sigma_h \Sigma_i I_i(h)$ where i are the independent observations of reflection h.

[b] R_{free} was calculated from 5% of the data, which were removed at random before the refinement was carried out.

[c] Refined atoms in the asymmetric unit.

diffraction data were collected at the beam line BL14.2 (BESSY, Berlin, Germany). All diffraction data were processed and scaled using the XDS package.[45] The structures were solved using difference Fourier techniques with the isomorphous structure of XenA$_{ox}$ determined at 1.5 Å.[6] Subsequent rounds of model building and refinement were performed using the programs Coot[46] and PHENIX.[47] The structures at true atomic resolution (d_{min} <1.2 Å) were refined as models with riding hydrogen atoms and included anisotropic *B*-factors.

Protein Data Bank accession numbers

The coordinates and structure factor amplitudes have been deposited in the RCSB Protein Data Bank with ID codes *3L5L* (XenA-wt), *3L5M* (XenA-wt with coumarin), *3L67* (XenA-C25S), *3L68* (XenA-C25S with coumarin), *3L65* (XenA-C25A) and *3L66* (XenA-C25A with coumarin).

Supplementary Data

Supplementary data associated with this article can be found, in the online version, at doi:10.1016/j.jmb.2010.02.044

References

1. Williams, R. E. & Bruce, N. C. (2002). 'New uses for an old enzyme'–the old yellow enzyme family of flavoenzymes. *Microbiology*, **148**, 1607–1614.
2. Brige, A., Van den Hemel, D., Carpentier, W., De Smet, L. & Van Beeumen, J. J. (2006). Comparative characterization and expression analysis of the four old yellow enzyme homologues from *Shewanella oneidensis* indicate differences in physiological function. *Biochem. J.* **394**, 335–344.
3. Niino, Y. S., Chakraborty, S., Brown, B. J. & Massey, V. (1995). A new old yellow enzyme of *Saccharomyces cerevisiae*. *J. Biol. Chem.* **270**, 1983–1991.
4. van Dillewijn, P., Wittich, R. M., Caballero, A. &

Ramos, J. L. (2008). Subfunctionality of hydride transferases of the old yellow enzyme family of flavoproteins of *Pseudomonas putida*. *Appl. Environ. Microbiol.* **74**, 6703–6708.

5. Fetzner, S., Tshisuaka, B., Lingens, F., Kappl, R. & Huttermann, J. (1998). Bacterial degradation of quinoline and derivatives – pathways and their biocatalysts. *Angew. Chem. Int. Ed.* **37**, 577–597.

6. Griese, J. J., P Jakob, R., Schwarzinger, S. & Dobbek, H. (2006). Xenobiotic reductase A in the degradation of quinoline by *Pseudomonas putida* 86: physiological function, structure and mechanism of 8-hydroxycoumarin reduction. *J. Mol. Biol.* **361**, 140–152.

7. Fox, K. M. & Karplus, P. A. (1994). Old yellow enzyme at 2 Å resolution: overall structure, ligand binding, and comparison with related flavoproteins. *Structure*, **2**, 1089–1105.

8. Barna, T., Messiha, H. L., Petosa, C., Bruce, N. C., Scrutton, N. S. & Moody, P. C. (2002). Crystal structure of bacterial morphinone reductase and properties of the C191A mutant enzyme. *J. Biol. Chem.* **277**, 30976–30983.

9. Barna, T. M., Khan, H., Bruce, N. C., Barsukov, I., Scrutton, N. S. & Moody, P. C. (2001). Crystal structure of pentaerythritol tetranitrate reductase: "flipped" binding geometries for steroid substrates in different redox states of the enzyme. *J. Mol. Biol.* **310**, 433–447.

10. Khan, H., Barna, T., Harris, R. J., Bruce, N. C., Barsukov, I., Munro, A. W. *et al.* (2004). Atomic resolution structures and solution behavior of enzyme-substrate complexes of *Enterobacter cloacae* PB2 pentaerythritol tetranitrate reductase. Multiple conformational states and implications for the mechanism of nitroaromatic explosive degradation. *J. Biol. Chem.* **279**, 30563–30572.

11. van den Hemel, D., Brige, A., Savvides, S. N. & Van Beeumen, J. (2006). Ligand-induced conformational changes in the capping subdomain of a bacterial old yellow enzyme homologue and conserved sequence fingerprints provide new insights into substrate binding. *J. Biol. Chem.* **281**, 28152–28161.

12. Kitzing, K., Fitzpatrick, T. B., Wilken, C., Sawa, J., Bourenkov, G. P., Macheroux, P. & Clausen, T. (2005). The 1.3 Å crystal structure of the flavoprotein YqjM reveals a novel class of old yellow enzymes. *J. Biol. Chem.* **280**, 27904–27913.

13. Spiegelhauer, O., Dickert, F., Mende, S., Niks, D., Hille, R., Ullmann, M. & Dobbek, H. (2009). Kinetic characterization of xenobiotic reductase A from *Pseudomonas putida* 86. *Biochemistry*, **48**, 11412–11420.

14. Khan, H., Harris, R. J., Barna, T., Craig, D. H., Bruce, N. C., Munro, A. W. *et al.* (2002). Kinetic and structural basis of reactivity of pentaerythritol tetranitrate reductase with NADPH, 2-cyclohexenone, nitroesters, and nitroaromatic explosives. *J. Biol. Chem.* **277**, 21906–21912.

15. Messiha, H. L., Bruce, N. C., Sattelle, B. M., Sutcliffe, M. J., Munro, A. W. & Scrutton, N. S. (2005). Role of active site residues and solvent in proton transfer and the modulation of flavin reduction potential in bacterial morphinone reductase. *J. Biol. Chem.* **280**, 27103–27110.

16. Stewart, R. C. & Massey, V. (1985). Potentiometric studies of native and flavin-substituted old yellow enzyme. *J. Biol. Chem.* **260**, 13639–13647.

17. Xu, D., Kohli, R. M. & Massey, V. (1999). The role of threonine 37 in flavin reactivity of the old yellow enzyme. *Proc. Natl Acad. Sci. USA*, **96**, 3556–3561.

18. Bougioukou, D. J., Kille, S., Taglieber, A. & Reetz, M. T. (2009). Directed evolution of an enantioselective enoate-reductase: testing the utility of iterative saturation mutagenesis. *Adv. Synth. Catal.* **351**, 3287–3305.

19. Abramovitz, A. S. & Massey, V. (1976). Interaction of phenols with old yellow enzyme. Physical evidence for charge-transfer complexes. *J. Biol. Chem.* **251**, 5327–5336.

20. Craig, D. H., Moody, P. C., Bruce, N. C. & Scrutton, N. S. (1998). Reductive and oxidative half-reactions of morphinone reductase from *Pseudomonas putida* M10: a kinetic and thermodynamic analysis. *Biochemistry*, **37**, 7598–7607.

21. Fitzpatrick, T. B., Amrhein, N. & Macheroux, P. (2003). Characterization of YqjM, an old yellow enzyme homolog from *Bacillus subtilis* involved in the oxidative stress response. *J. Biol. Chem.* **278**, 19891–19897.

22. Berkholz, D. S., Faber, H. R., Savvides, S. N. & Karplus, P. A. (2008). Catalytic cycle of human glutathione reductase near 1 Å resolution. *J. Mol. Biol.* **382**, 371–384.

23. Breinlinger, E. C., Keenan, C. J. & Rotello, V. M. (1998). Modulation of flavin recognition and redox properties through donor atom-π interactions. *J. Am. Chem. Soc.* **120**, 8606–8609.

24. Ghisla, S. & Massey, V. (1986). New flavins for old: artificial flavins as active site probes of flavoproteins. *Biochem. J.* **239**, 1–12.

25. Bruice, T. C. & Benkovic, S. J. (2000). Chemical basis for enzyme catalysis. *Biochemistry*, **39**, 6267–6274.

26. Bruice, T. C. & Pandit, U. K. (1960). Intramolecular models depicting the kinetic importance of "fit" in enzymatic catalysis. *Proc. Natl Acad. Sci. USA*, **46**, 402–404.

27. Jencks, W. P. (1963). Mechanism of enzyme action. *Annu. Rev. Biochem.* **32**, 639–676.

28. Fraaije, M. W. & Mattevi, A. (2000). Flavoenzymes: diverse catalysts with recurrent features. *Trends Biochem. Sci.* **25**, 126–132.

29. Wessjohann, L. A., Schneider, A., Abbas, M. & Brandt, W. (2007). Selenium in chemistry and biochemistry in comparison to sulfur. *Biol. Chem.* **388**, 997–1006.

30. Jimenez, J. I., Minambres, B., Garcia, J. L. & Diaz, E. (2002). Genomic analysis of the aromatic catabolic pathways from *Pseudomonas putida* KT2440. *Environ. Microbiol.* **4**, 824–841.

31. Sambrook, J. & Russel, D. (2001). *Molecular Cloning: A Laboratory Manual.* Cold Spring Harbor Laboratory Press Cold Spring Harbor, NY.

32. Aliverti, A., Curti, B. & Vanoni, M. A. (1999). Identifying and quantitating FAD and FMN in simple and in iron-sulfur-containing flavoproteins. *Methods Mol. Biol.* **131**, 9–23.

33. Massey, V., Stankovich, M. & Hemmerich, P. (1978). Light-mediated reduction of flavoproteins with flavins as catalysts. *Biochemistry*, **17**, 1–8.

34. Sucharitakul, J., Chaiyen, P., Entsch, B. & Ballou, D. P. (2005). The reductase of p-hydroxyphenylacetate 3-hydroxylase from *Acinetobacter baumannii* requires p-hydroxyphenylacetate for effective catalysis. *Biochemistry*, **44**, 10434–10442.

35. Loach, P. A. (1973). Oxidation-reduction potentials: absorbance bands and molar absorbance of compounds used in biochemical studies. In *Handbook of Biochemistry Selected Data for Molecular Biology* (Sorber, H. A., ed.), pp. J33–J40, CRC Press, Cleveland, OH.

36. Efimov, I. & McIntire, W. S. (2004). A study of the spectral and redox properties and covalent flavinylation of the flavoprotein component of p-cresol methylhydroxylase reconstituted with FAD analogues. *Biochemistry*, **43**, 10532–10546.

37. Strickland, S., Palmer, G. & Massey, V. (1975). Determination of dissociation constants and specific rate constants of enzyme-substrate (or protein-ligand) interactions from rapid reaction kinetic data. *J. Biol. Chem.* **250**, 4048–4052.

38. Essigke, T. (2008). *A continuum electrostatic approach for calculating the binding energetics of multiple ligans.* Dissertation, Universität Bayreuth.

39. Ullmann, G. M. & Knapp, E. W. (1999). Electrostatic models for computing protonation and redox equilibria in proteins. *Eur. Biophys. J.* **28**, 533–551.

40. Bashford, D. & Gerwert, K. (1992). Electrostatic calculations of the pK_a values of ionizable groups in bacteriorhodopsin. *J. Mol. Biol.* **224**, 473–486.

41. MacKerell, A. D., Bashford, D., Bellott, M., Dunbrack, R. L., Jr, Evanseck, J. D., Field, M. J. *et al.* (1998). All-atom empirical potential for molecular modeling and dynamics studies of proteins. *J. Phys. Chem. B*, **102**, 3586–3616.

42. Bashford, D., Case, D. A., Dalvit, C., Tennant, L. & Wright, P. E. (1993). Electrostatic calculations of side-chain pKa values in myoglobin and comparison with NMR data for histidines. *Biochemistry*, **32**, 8045–8056.

43. TeVelde, G., Bickelhaupt, F. M., Baerends, E. J., Guerra, C. F., VanGisbergen, S. J. A., Snijders, J. G. & Ziegler, T. (2001). Chemistry with ADF. *J. Comput. Chem.* **22**, 931–967.

44. Klapper, I., Hagstrom, R., Fine, R., Sharp, K. & Honig, B. (1986). Focusing of electric fields in the active site of Cu-Zn superoxide dismutase: effects of ionic strength and amino-acid modification. *Proteins: Struct. Funct. Genet.* **1**, 47–59.

45. Kabsch, W. (1988). Automatic indexing of rotation diffraction patterns. *J. Appl. Crystalog.* **21**, 67–71.

46. Emsley, P. & Cowtan, K. (2004). Coot: model-building tools for molecular graphics. Acta Crystallogr. *D*, **60**, 2126–2132.

47. Adams, P. D., Grosse-Kunstleve, R. W., Hung, L. W., Ioerger, T. R., McCoy, A. J., Moriarty, N. W. *et al.* (2002). PHENIX: building new software for automated crystallographic structure determination. *Acta Crystallogr. D*, **58**, 1948–1954.